



Cite this: *Phys. Chem. Chem. Phys.*, 2025, 27, 4959

# Single-chirality single-wall carbon nanotubes for electrochemical biosensing†

Ju-Yeon Seo,<sup>a</sup> Bahar Mostafiz,<sup>a</sup> Xiaomin Tu,<sup>c</sup> Constantine Y. Khripin,<sup>c</sup> Ming Zheng,<sup>c</sup> Han Li<sup>\*ab</sup> and Emilia Peltola<sup>\*a</sup>

Single-wall carbon nanotubes (SWCNTs) exhibit versatile optoelectronic properties closely linked to their structural characteristics, such as chiral angles and diameters. Given this, they are promising materials for biosensors. However, in studies investigating SWCNT-based electrochemical biosensors, raw soot has been mostly used. Soot typically contains a mixture of different chiralities, metallic compounds, and various impurities from the synthesis process. As a result, this mixture significantly limits the reproducibility and precision of SWCNT-based sensors. To ensure consistent sensor performance, we employed an aqueous two-phase extraction (ATPE) technique to purify and sort single-chirality SWCNTs—specifically, semiconducting (6,5) SWCNTs and metallic (6,6) SWCNTs. In addition, we used multiple fabrication methods to ensure that only pure-chirality SWCNTs were deposited onto the electrodes. Our findings emphasise the importance of using surfactant-free systems when investigating the influence of chirality on the electrochemical behaviour of SWCNTs. By using monochiral SWCNTs, we achieved precise control over their concentration and density, allowing us to assess their electrochemical properties accurately. Our results reveal that the adsorption-controlled process of the inner sphere redox probe occurs on (6,5) SWCNTs, while a diffusion-controlled process is observed on (6,6) SWCNTs. These findings provide valuable insights that will enhance the performance of SWCNT-based electrochemical biosensors.

Received 4th November 2024,  
 Accepted 8th February 2025

DOI: 10.1039/d4cp04206a

rsc.li/pccp

## 1. Introduction

Carbon nanotubes (CNTs) have been widely investigated in various applications because of their unique optoelectronic properties.<sup>1</sup> CNT-based electrochemical sensors exhibit higher sensitivity and faster electron kinetics than traditional carbon-based electrode materials such as graphene and carbon nanofibers.<sup>2,3</sup> CNT-based electrodes facilitate the direct electrochemical transfer between biorecognition elements without electronic media or a promotor, acting as molecular wires between the active sites of biorecognition elements and electrode surfaces.<sup>4,5</sup> Furthermore, CNT-modified electrodes can alleviate surface fouling, such as processes involved in NADH oxidation.<sup>6–8</sup>

CNT-based biosensors can be based on multi-wall carbon nanotubes (MWCNTs) or single-wall carbon nanotubes

(SWCNTs). Compared to MWCNTs, SWCNTs demonstrate strong antimicrobial activity as the diameter decreases,<sup>9,10</sup> and exhibit distinctive electrochemical properties due to their quasi-one-dimensional quantum effect.<sup>11,12</sup>

The properties of SWCNTs are highly dependent on their structure and chirality, which determine their electronic band structure.<sup>13</sup> Chirality in SWCNTs refers to how the graphene sheet is rolled to form the cylindrical structure of the nanotube. The nanotube's chirality, or “twist”, can be described by a pair of indices ( $n, m$ ) known as the chiral vector, denoted as  $C = na_1 + ma_2$ , where  $a_1$  and  $a_2$  are lattice unit vectors. Based on their chirality, SWCNTs can be metallic or semiconducting.<sup>14</sup> However, most biosensor studies have utilised raw soot or unsorted SWCNTs,<sup>4,15,16</sup> limiting the full exploration of their potential. Due to the chirality- and structure-dependent properties of SWCNTs, the sensitivity and selectivity of their biosensors can vary significantly,<sup>4,17</sup> making it challenging to interpret sensing mechanisms.<sup>18</sup> For example, Pumera's group observed that metallic SWCNTs exhibited better electrochemical properties than semiconducting SWCNTs, although the specific chiralities of SWCNTs were not investigated.<sup>19</sup> Additionally, single-chirality (6,5) SWCNTs have shown enantioselective recognition of DOPA using both square wave voltammetry and differential pulse voltammetry techniques.<sup>20–24</sup> However, to our knowledge,

<sup>a</sup> Department of Mechanical and Materials Engineering, University of Turku, Turku, FI-20014, Finland. E-mail: emilia.peltola@utu.fi

<sup>b</sup> Turku Collegium for Science, Medicine and Technology, University of Turku, Turku, FI-20520, Finland. E-mail: han.li@utu.fi

<sup>c</sup> Materials Science and Engineering Division, National Institute of Standard and Technology, Gaithersburg, MD, 20899, USA

† Electronic supplementary information (ESI) available. See DOI: <https://doi.org/10.1039/d4cp04206a>



there has not yet been a comparative study of electrochemical sensors that utilise SWCNTs with varying chiralities and distinct electronic properties. In this paper, we first separate single-chirality SWCNTs, specifically the semiconducting (6,5) and metallic (6,6) types, using an aqueous two-phase extraction technique (ATPE).<sup>25,26</sup> Compared with other commonly used sorting techniques, the ATPE method offers greater scalability while still achieving high purity.<sup>27</sup> This is crucial for obtaining sufficient quantities for each chirality, particularly (6,6) type in this work, for electrode fabrication and comparative electrochemical studies. We first prepare standalone electrodes to confirm the electrochemical responses of single-chirality SWCNTs without an electrochemically conductive substrate. Additionally, we fabricate the electrochemical sensors modified with (6,6) and (6,5) SWCNTs by drop-casting and vacuum-filtered thin film transfer onto screen-printed carbon electrodes (SPCEs). Through a concentration study of (6,5) and (6,6) SWCNTs thin film-modified SPCEs, we determine the optimal concentration of SWCNTs for these applications. The outer sphere redox (OSR) and the inner sphere redox (ISR) probe processes were used to investigate the surface characteristics and the material's sensitivity. The results demonstrate the importance of maintaining a surfactant-free surface and underscore that the electrochemical sensing mechanism is dependent on the chirality of the SWCNTs. These findings emphasise the crucial role of chirality in defining the electrochemical sensing capabilities of SWCNTs.

## 2. Experimental section

Certain equipment, instruments or materials are identified in this paper in order to adequately specify the experimental details. Such identification does not imply recommendation by the National Institute of Standards and Technology (NIST), nor does it imply the materials are necessarily the best available for the purpose.

### 2.1. Materials and apparatus

(6,6) and (6,5) SWCNTs were prepared from a raw (6,5) chirality-enriched SWCNTs mixture (CoMoCat SG65i *via* Sigma-Aldrich) to fabricate SWCNTs modified SPCEs and standalone SWCNTs electrodes. SPCEs (DropSens C110, Metrohm, Spain) were used as substrates to fabricate the modified electrodes. SPCEs incorporate an electrode system consisting of a carbon working electrode (4 mm diameter), a carbon counter electrode, and an Ag pseudo reference electrode. Dopamine hydrochloride(4-(2-aminoethyl) benzene-1,2-diol hydrochloride, Sigma-Aldrich, 98%) and hexaamineruthenium(III) chloride (azane;ruthenium;trichloride, Sigma-Aldrich, 98%) were used to prepare the solutions for electrochemical measurements.

### 2.2. Preparation of the suspension of chirality pure SWCNTs (ATPE method)

As previously established and detailed in earlier studies,<sup>25,28</sup> the isolation of SWCNTs with chiralities (6,6) and (6,5) was

accomplished using an (ATPE) approach. A 30 mg sample of a raw (6,5) chirality-enriched SWCNT mixture (Sigma-Aldrich) was suspended in 30 mL of aqueous 10 g L<sup>-1</sup> (1% mass/volume) sodium deoxycholate (DOC, BioChemica) by tip sonication (Ultrasonic Homogenizer, FS-750T) for 45 minutes while immersed in an ice bath. The resulting dispersion was then centrifuged (Eppendorf 5810) at 16 639 g for 1 hour, and the supernatant was collected for further ATPE sorting. The ATPE was carried out in a solution of dextran (MW 70 000 Da, TCI) and polyethylene glycol (PEG, MW 6000 Da, Sigma-Aldrich). For diameter sorting of the (6,6), the DOC concentration was maintained at a fixed 0.05% m/v, and the sodium dodecyl sulfate (SDS, Sigma-Aldrich) concentration increases from 0.7% to 1% m/v to collect all (6,6) SWCNTs in the PEG phase. For the (6,5) chirality, the SDS concentration was adjusted between 1.3% and 1.5% m/v (Sigma-Aldrich) to achieve selective isolation. Subsequently, a semiconducting-metallic sorting step was applied to both chiralities as previously described.<sup>28</sup> This step involved adjusting the overall surfactant concentrations to 0.9% sodium cholate (SC, Sigma-Aldrich), 1% SDS, and less than 0.02% DOC. Sodium hypochlorite (NaClO, 10–15% available chlorine, Honeywell) was then added at 5  $\mu$ L mL<sup>-1</sup> of a solution, pre-diluted to a 1/100th concentration in water, to facilitate the semiconducting-metallic separation. All sorted species were reconcentrated to 1% DOC (m/v) through iterative concentration and dilution cycles in a pressurised ultrafiltration stirred cell (Millipore) equipped with a 300 kDa cutoff membrane.

### 2.3. Fabrication of the electrochemical sensors

SPCEs were modified by drop casting single-chirality SWCNTs and by transferring single-chirality SWCNTs thin film (For a visual representation, see Fig. S1 in the ESI†). The concentrations of both (6,5) and (6,6) SWCNTs were carefully adjusted for comparison. The ESI,† provides detailed calculations in Section E, including Table S2 (ESI†). The surface modification of SPCEs was carried out following the protocol established by Ishizaki *et al.*<sup>29</sup> The aqueous dispersion solution containing (6,5) and (6,6) SWCNTs was vacuum filtered through the PTFE membrane (Cytiva, pore size 0.2  $\mu$ m) and the surfactants were washed away. An annealing step (90 °C) was conducted to dry the solvent after drop casting and to transfer the SWCNTs to SPCEs. For the fabrication of standalone single-chirality SWCNTs electrodes, Corning® Plain Micro Slides (Corning, NY, USA) were sonicated in ethanol for 10 minutes, and an ethanol-wetted SWCNT film was press transferred to the Corning® Plain Micro Slides on a hot plate. Conductive silver paste (Electrolube) was added to provide electronic contact between a conductive copper sheet and the SWCNT films following the protocol by Rantataro *et al.*<sup>30</sup> Additionally, a conductive copper tape was used to contact the silver paste to the micro slides with single-chirality SWCNTs. The electrodes were then insulated with polytetrafluoroethylene tape, exposing only a 4 mm diameter hole. This hole was aligned directly above the micro slides with single-chirality SWCNTs.



#### 2.4. Material characterisation

The absorption spectra were recorded using the Specord 200 Plus UV-vis spectrophotometer to determine the chirality of SWCNTs. The cuvette path length was 1 cm, and the measured wavelength was 190 to 1100 nm. Thermo Scientific Apreo S. Field-emission scanning electron microscope at 2 kV accelerating voltage was used for imaging the (6,5) and (6,6) SWCNTs drop casted SPCEs and (6,5) and (6,6) SWCNTs thin film/SPCEs. Surface chemical analysis of (6,5) SWCNTs drop casted SPCE and (6,5) SWCNTs thin film/SPCE was conducted using Thermo Scientific Nexsa X-ray photoelectron spectrometer (XPS) System to verify the presence of surfactants. The samples were placed under a vacuum overnight, and an Al K $\alpha$  X-ray source ( $h\nu = 1486.6$  eV) was used for the measurements. The XPS survey was carried out with an energy step of 1 eV at 200 eV pass energy. High-resolution spectra were recorded at 0.1 eV step and 50 eV pass energy. Binding energy scale calibration was based on carbon C 1s C–C peak at 284.8 eV binding energy. Resistivity, sheet resistance, and conductivity of  $2 \mu\text{g cm}^{-2}$  (6,5) and (6,6) SWCNTs on Corning<sup>®</sup> Plain Micro Slides were measured by an Ossila four-point probe system. 101 readings from 3 locations were obtained to avoid the potential bias. The thickness of (6,5) and (6,6) SWCNTs was compared by an atomic force microscope (AFM). AFM measurements were performed with Park Systems NX10 in a tapping mode using a Bruker NCHV probe. The XEI software was used to determine the step-height profile (thickness). The AFM samples were prepared on silicon wafers with a density of  $2 \mu\text{g cm}^{-2}$  for (6,5) and (6,6) SWCNTs.

#### 2.5. Electrochemical characterisation

Cyclic voltammetry was carried out using a Gamry reference potentiostat 600. DropSens C110 (SPCE) consists of three components: a carbon working electrode, a carbon counter electrode, and a silver (Ag) reference electrode. SPCEs were used to prepare SWCNTs drop casted SPCEs and SWCNTs thin film/SPCEs. A universal sensor connector was used for SWCNTs drop casted SPCEs. A three-electrode cell was used for standalone SWCNTs electrodes and SWCNTs thin film/SPCEs. Cyclic voltammetry measurements for standalone SWCNTs electrodes and SWCNTs thin film/SPCEs were conducted using an Ag/AgCl reference electrode and a platinum wire as a counter electrode. A phosphate buffer saline (PBS) solution was prepared by dissolving 80 g NaCl (> 99%, Sigma Aldrich), 2.0 g KCl (VWR), 14.4 g Na<sub>2</sub>HPO<sub>4</sub> (Merck), and 2.4 g KH<sub>2</sub>PO<sub>4</sub> (VWR) in 10 L of deionised water (resistivity 18.2 M $\Omega$  cm, Milli-Q, Millipore, Billerica MA) with a final pH of 7.4. The measurements were carried out in 1 mM Ru(NH<sub>3</sub>)<sub>6</sub><sup>2+/3+</sup> in 1 M KCl, 50  $\mu\text{M}$  DA in PBS, and concentration series (DA 0.05  $\mu\text{M}$ –100  $\mu\text{M}$ ) in PBS by (6,5) and (6,6) SWCNTs thin film/SPCE.

Oxygen can be reduced at the working electrode and induce DA-self polymerisation.<sup>31,32</sup> This can be avoided by purging with nitrogen or argon for 15–30 minutes.<sup>31</sup> Therefore, oxygen in the solutions was removed by purging with N<sub>2</sub> for at least 15 minutes before the measurement, and the N<sub>2</sub> channel was kept above the solution throughout the experiments.

### 3. Results and discussion

#### 3.1. Chemical characterisation

Fig. 1 shows the absorption spectra of chirality-sorted SWCNTs. Semiconducting (6,5) SWCNTs present two optical transition peaks (S<sub>11</sub>, S<sub>22</sub>) in the absorption spectrum where S<sub>11</sub> and S<sub>22</sub> appear at 989 nm and 572 nm, respectively. The metallic (6,6) SWCNTs showed the peak absorbance (M<sub>11</sub>) at the wavelength of 456 nm. The results confirm the successful separation of (6,5) and (6,6) SWCNTs. Determining the molar concentration of SWCNTs in solution has been challenging due to their varying structure and insolubility. Also, insufficient experimental data hindered studying factors affecting the supermolecular association of SWCNTs.<sup>33</sup> As discussed in ESI<sup>†</sup>, the extinction coefficients were determined using size-exclusion chromatography (SEC) for DNA quantification using purified single-chirality DNA-SWCNT hybrids.<sup>34</sup> This information was needed to fabricate electrodes with an equal density of (6,6) and (6,5) SWCNTs. As shown in Fig. S5 (ESI<sup>†</sup>), we further investigated the impact of SWCNTs concentration by comparing peak anodic current (*i*<sub>p,a</sub>). The density for standalone SWCNTs electrodes, SWCNTs drop casted SPCEs, and SWCNTs thin film/SPCEs was fixed to be  $2 \mu\text{g cm}^{-2}$ .

#### 3.2. Four-point probe measurements

As shown in Table S1 (ESI<sup>†</sup>), the sheet resistance and conductivity of (6,5) and (6,6) SWCNTs vary significantly due to their semiconducting and metallic properties, with differences of roughly 300 times. Specifically, (6,5) SWCNTs exhibited a sheet resistance of 1387311  $\Omega \text{sq}^{-1}$  and a conductivity of 3.7 S m<sup>-1</sup>. In contrast, (6,6) SWCNTs showed a sheet resistance of 4868  $\Omega \text{sq}^{-1}$  and a conductivity of 1092 S m<sup>-1</sup>.

Overall, metallic CNTs exhibit excellent electrical conductivity, facilitating efficient electron transfer between the analyte and the electrode surface. In contrast, the electron transfer capabilities of semiconductive CNTs are constrained by their bandgap and often require external doping or electrochemical

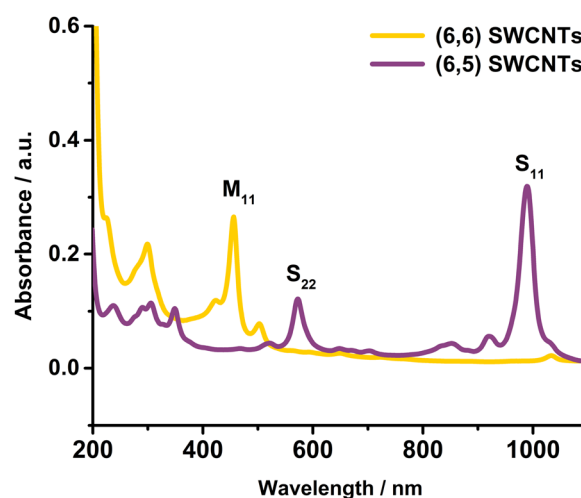


Fig. 1 Absorption spectra of suspension of single-chirality (6,5) and (6,6) SWCNTs.



activation to improve conductivity. However, when either type of SWCNT is applied as a thin film on a conductive electrode surface, the analyte-surface interactions become the primary determinant of electrochemical performance, as reflected by the similar peak current from the cyclic voltammetry measurements.

### 3.3. Surface characterisation

Fig. 2 presents the surface comparison of (6,5) SWCNTs and (6,6) SWCNTs drop casted SPCEs and (6,5) and (6,6) SWCNTs thin film/SPCEs. As shown in Fig. 2A, sodium deoxycholate (DOC) is placed in the centre of working electrodes, whereas the (6,5) and (6,6) SWCNTs were situated on their rim (Fig. S2, ESI<sup>†</sup>). In contrast, Fig. 2B and D show a well-exposed SWCNTs network without DOC. We used the vacuum-filtered SWCNTs films to fabricate the standalone electrodes and modify the SPCEs' surface for the following measurements. The complete removal of the surfactant was verified with XPS, showing that the Na-peak from the surfactant is pronounced in (6,5) SWCNTs drop casted SPCE, but non-existent in (6,5) SWCNTs thin film/SPCE (Fig. S3, ESI<sup>†</sup>). The thickness of  $2 \mu\text{g cm}^{-2}$  (6,5) and (6,6) SWCNTs was compared by AFM measurements. As shown in Fig. S4 (ESI<sup>†</sup>), their thickness was determined to be roughly 40 nm (Table S3, ESI<sup>†</sup>), which is consistent with the thickness observed in previous studies using the same concentration of SWCNTs.<sup>35</sup>

### 3.4. Electrochemical characterisation

Cyclic voltammetry was used to study the electrochemical properties of single-chirality SWCNTs with three types of electrodes, evaluating surface area, electron transfer kinetics, and ISR probe reactions, which are particularly surface-sensitive. These reactions provide critical insights into the interfacial properties, as the ISR species directly interact with the electrode surface. The insights gained are crucial for optimising direct electrochemical detection of biological molecules.

#### 3.4.1. Standalone single-chirality SWCNTs electrodes.

Standalone SWCNTs electrodes were fabricated to investigate

the intrinsic properties of single-chirality SWCNTs, eliminating the influence of the conductive substrate. Fig. 3 displays the electrochemical properties of semiconducting (6,5) and metallic (6,6) SWCNTs using the OSR,  $\text{Ru}(\text{NH}_3)_6^{3+/2+}$ , and the ISR species, DA. In Fig. 3A and C, standalone (6,5) SWCNTs electrode demonstrates lower electron transfer kinetics compared to its metallic counterpart (6,6) SWCNTs (Fig. 3B and D). Semiconducting SWCNTs, such as (6,5) chirality, have reduced electrical conductivity at room temperature, which can limit their electrochemical performance when used as standalone electrodes.<sup>36,37</sup> Overall, the cyclic voltammograms of the standalone (6,6) SWCNTs electrode exhibit approximately ten times higher currents than those of the standalone (6,5) SWCNTs electrode for both OSR and ISR reactions. This significant difference highlights the impact of the intrinsic electronic properties of single-chirality SWCNTs on their electrochemical behaviour, as well as the effectiveness of the sorting process in producing high-purity, well-defined SWCNT suspensions.

#### 3.4.2. Single-chirality SWCNTs drop casted SPCEs

Single-chirality SWCNTs drop casted electrodes were first measured to compare their electrochemical behaviour of single-chirality SWCNTs on SPCEs. For drop casting methods, a surfactant such as DOC is essential.

Fig. 4 shows insignificant differences between the drop casted electrodes in electron transfer kinetics and current intensity towards 1 mM OSR,  $\text{Ru}(\text{NH}_3)_6^{3+/2+}$  and 50  $\mu\text{M}$  ISR, DA. Surfactants are indispensable for stable and homogeneous dispersions of SWCNTs in an aqueous solution.<sup>38</sup> Surfactants were anticipated to impact electrochemical characterisation, as shown in Fig. S6 and S7 (ESI<sup>†</sup>). These figures compare bare SPCE and 1% DOC drop casted electrodes, along with (6,5) and (6,6) SWCNTs drop casted electrodes, for OSR 1 mM and ISR 50  $\mu\text{M}$ . As shown by Fig. 4A, for OSR, the difference between only DOC 1% (w/v), (6,5) and (6,6) SWCNTs drop casted SPCEs is negligible. All drop casted electrodes showed an average  $\Delta E_p$  of 56 mV and an average oxidation peak current of 29.5  $\mu\text{A}$ . For ISR, the average of  $\Delta E_p$  was 27 mV, and the average oxidation peak current was 3.8  $\mu\text{A}$ . The presence of 1% DOC masked any potential impact from the SWCNTs, and the chirality impact could not be observed. Although drop casting is a common and straightforward technique for fabricating SWCNT-modified electrodes, the surfactants used in SWCNT suspensions can form a layer over the SWCNT networks.<sup>39</sup> This surfactant layer can hinder the direct observation of chirality-dependent differences in the SWCNTs' electrochemical behaviours.

#### 3.4.2. Single-chirality SWCNTs thin film/SPCEs

Single-chirality SWCNTs thin film/SPCEs were prepared to overcome the limitations associated with surfactant-covered SWCNTs thin films produced by drop casting. We introduced a thin-film transfer method to fabricate surfactant-free SWCNTs-films on SPCEs, which were used as a substrate to facilitate the electron flow of both (6,6) and (6,5) SWCNTs. This approach allows us to study the intrinsic electrochemical

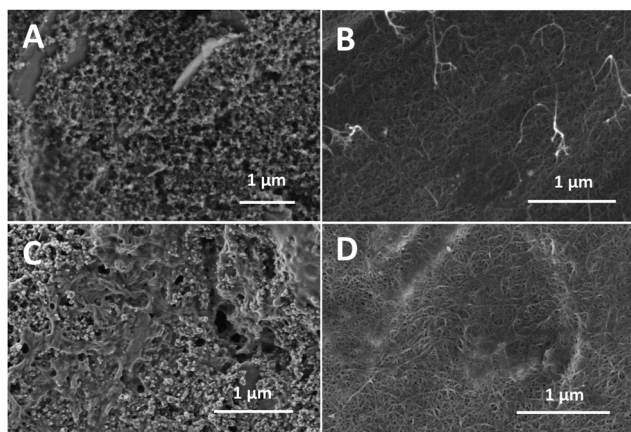


Fig. 2 (A) (6,5) SWCNTs drop casted SPCE, (B) (6,5) SWCNTs thin film/SPCE, (C) (6,6) SWCNTs drop casted SPCE, (D) (6,6) SWCNTs thin film/SPCE.



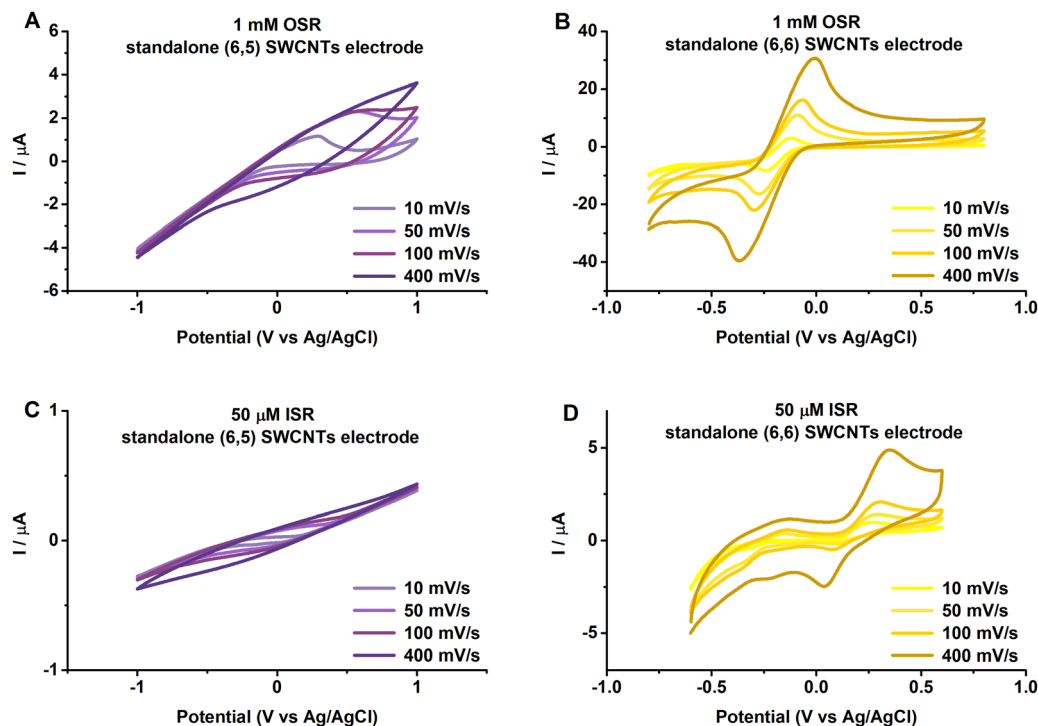


Fig. 3 Cyclic voltammograms of standalone SWCNTs electrodes with varying scan rates 10–400  $\text{mV s}^{-1}$ , in (A) and (C) 1 mM  $\text{Ru}(\text{NH}_3)_6^{3+/2+}$  in 1 M KCl and (B) and (D) DA 50  $\mu\text{M}$  in PBS.

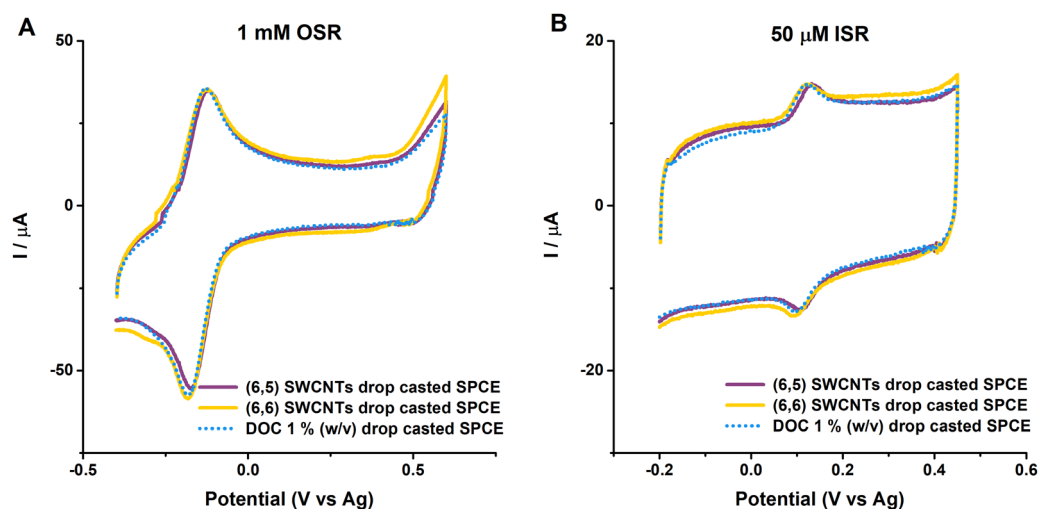


Fig. 4 Cyclic voltammograms of SWCNTs drop casted SPCEs with a scan rate of 100  $\text{mV s}^{-1}$ , in (A) 1 mM  $\text{Ru}(\text{NH}_3)_6^{3+/2+}$  in 1 M KCl and (B) DA 50  $\mu\text{M}$  in PBS.

properties of single-chirality SWCNTs without the interference of surfactants.

Fig. 5 presents average cyclic voltammograms from three measurements using SWCNTs thin film/SPCEs modified with (6,5) or (6,6) SWCNTs, highlighting the distinct electrochemical behaviours of OSR and ISR probes. For the OSR probe,  $\text{Ru}(\text{NH}_3)_6^{3+/2+}$ , minimal differences were observed between bare SPCEs or SWCNTs thin film/SPCEs regarding peak currents and peak-to-peak separation ( $\Delta E_p$ , Table 1). The electron transfer

process of the OSR by SWCNTs thin film/SPCEs is governed by diffusion control, and the peak current ( $i_{p,c}$  and  $i_{p,a}$ ) can be used to calculate the electrochemically active surface area (ECSA or EASA) *via* Randles-Sevcik equation.<sup>40</sup> Although the SWCNTs can potentially increase surface area, the ECSA calculations indicated that the difference is negligible. Despite the similar electrochemical responses in Fig. 5, (6,5) SWCNTs thin film/SPCEs exhibit larger capacitive currents than (6,6) SWCNTs thin film/SPCEs in 1 M KCl and PBS (Fig. S8, ESI†).



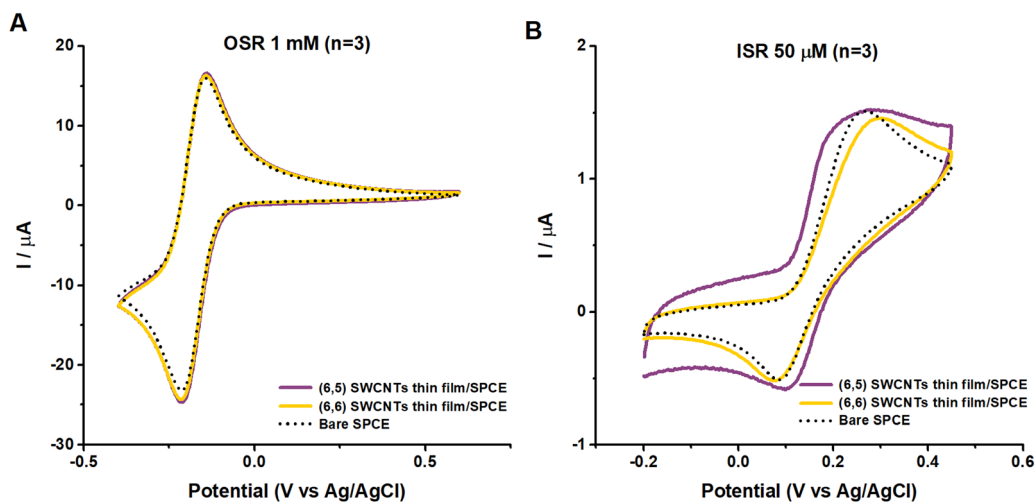


Fig. 5 Average of three cyclic voltammograms of SWCNTs thin film/SPCEs with a scan rate of  $100 \text{ mV s}^{-1}$  in (A)  $\text{Ru}(\text{NH}_3)_6^{3+/2+}$  1 mM in 1 M KCl and (B) DA  $50 \mu\text{M}$  in PBS.

Table 1 Results of the cyclic voltammetry measurements in 1 mM  $\text{Ru}(\text{NH}_3)_6^{3+/2+}$  in 1 M KCl at a scan rate of  $100 \text{ mV s}^{-1}$  ( $n = 3$ )

Sensor	$\Delta E_p$ (mV)	$i_{p,a}$ ( $\mu\text{A}$ )	$i_{p,c}$ ( $\mu\text{A}$ )	$i_{p,a}/i_{p,c}$
(6,5) SWCNTs thin film/SPCE	$74 \pm 2$	$20.8 \pm 0.8$	$23.5 \pm 1.4$	$0.88 \pm 0.06$
(6,6) SWCNTs thin film/SPCE	$73 \pm 1$	$21.1 \pm 1.5$	$23.9 \pm 1.2$	$0.88 \pm 0.08$
Bare SPCE	$71 \pm 3$	$20.7 \pm 0.6$	$22.9 \pm 0.4$	$0.91 \pm 0.03$

Previous research has also noticed that (6,5) SWCNTs have smaller diameters than (6,6) SWCNTs, resulting in higher electrostatic capacitance per unit length.<sup>41</sup>

When examining the ISR probe, DA  $50 \mu\text{M}$ , we found that the  $\Delta E_p$  slightly increased compared to the bare SPCEs, while the peak anodic current ( $i_{p,a}$ ) remained approximately the same (Table 2). Furthermore, significant differences emerged between the (6,5) and (6,6) SWCNTs thin film/SPCEs. The (6,5) SWCNTs thin film/SPCEs demonstrate a steep increase in current, indicating adsorption-dependent kinetics. The peak anodic current ( $i_{p,a}$ ) displays a distinct shoulder alongside the main peak (more visible at faster scan rates; see Fig. S9, ESI<sup>†</sup>), suggesting the presence of a secondary oxidation process. The shoulder oxidation peak appears at  $192 \text{ mV vs. Ag/AgCl}$ , and the prominent peak at  $278 \text{ mV vs. Ag/AgCl}$  with a scan rate of  $100 \text{ mV s}^{-1}$ .

Table 2 Results of the cyclic voltammetry measurements in  $50 \mu\text{M}$  DA in PBS at a scan rate of  $100 \text{ mV s}^{-1}$  ( $n = 3$ ). Log-plot slope was calculated from the peak anodic currents ( $i_{p,a}$ ) from  $400$  to  $50 \text{ mV s}^{-1}$ . Slopes of  $\log v$  vs.  $\log(i_{p,a})$  were calculated from <sup>1</sup>peak anodic currents at the shoulder and <sup>2</sup>main peak anodic currents

Sensor	$\Delta E_p$ (mV)	$i_{p,a}$ ( $\mu\text{A}$ )	Log-plot slope
(6,5) SWCNTs thin film/SPCE	$202 \pm 52$	$1.3 \pm 0.1$	$1^1, 0.5^2$
(6,6) SWCNTs thin film/SPCE	$223 \pm 39$	$1.4 \pm 0.1$	0.5
Bare SPCE	$179 \pm 25$	$1.5 \pm 0.1$	0.5

Notably, the overall DA reaction pathway can be described as an ECE (electrochemical-chemical-electrochemical) mechanism, with the secondary peak arising from the oxidation of leucodopaminechrome to dopaminechrome ( $\text{LDAC} \rightleftharpoons \text{DAC}$ ). In our case, the thin and permeable SWCNTs network likely facilitates initial DA oxidation at the (6,5) SWCNTs thin film/SPCEs ( $192 \text{ mV}$ ), followed by subsequent oxidation on the underlying SPCEs surface ( $278 \text{ mV}$ ).

We further analysed the reaction kinetics from the  $\log i_{p,a}$  vs.  $\log v$  plots, where a slope of 0.5 indicates a diffusion-controlled process, while a slope of 1 indicates an adsorption-controlled process. Diffusion-controlled behaviour suggests weak surface interactions, where the reaction rate is primarily determined by the transport of the analyte to the surface. In contrast, adsorption-controlled behaviour reflects strong surface interactions, with the material possessing active sites that bind the analyte tightly. (6,5) SWCNTs thin film/SPCEs showed adsorption-controlled behaviour for the shoulder oxidation peak towards DA (Table 2 and Fig. S9 in ESI<sup>†</sup>). The main peak anodic current, originating from the SPCE surface, had a slope of 0.5. In contrast, (6,6) SWCNTs thin film/SPCEs showed diffusion-controlled electrochemical behaviour with a slope of 0.5. In addition, the sensitivity of the (6,5) and (6,6) SWCNTs towards DA from  $0.05 \mu\text{M}$  to  $100 \mu\text{M}$  was nearly identical (Fig. S10, ESI<sup>†</sup>). The strong-surface interaction in adsorption-controlled behaviour results in a reliance on the availability and activity of these sites for detection. Such materials are particularly suited for detecting low-concentration analytes,



where strong and specific binding is critical for reliable detection.

By carefully tuning materials for adsorption-dependent kinetics, the selectivity of a biosensor for a specific analyte can be significantly enhanced. A clear example of such tuning has been demonstrated with carbon nanofibers (CNFs). The selectivity in this system is achieved through the following mechanisms: (i) when DA adsorbs onto CNFs, its oxidation peak shifts in the anodic direction, (ii) the adsorption of dehydroascorbic acid onto CNFs causes the oxidation peak of ascorbic acid to shift in the cathodic direction.<sup>42</sup> These opposing shifts increase the separation between the oxidation peaks of ascorbic acid and DA, allowing for improved discrimination between the two analytes.

As a simplification, adsorption-based materials are particularly effective for detecting rare or low-abundance analytes due to their specificity, whereas diffusion-based materials may be better suited for high-abundance analytes or applications requiring rapid response times.

### 3.5. Electrochemical sensing mechanism of (6,6) and (6,5) SWCNTs

In this study, we utilised metallic (6,6) and semiconductive (6,5) SWCNTs. When a SWCNT thin film is applied to a conductive electrode surface, analyte-surface interactions become the primary determinant of its electrochemical performance. Our proof-of-concept demonstrates that different chirality significantly influences the electrochemical sensing of ISR species.

Based on our observations, the different mechanisms of (6,5) and (6,6) SWCNTs towards DA can be explained by the structural characteristics of both single-chirality SWCNTs and DA. Typically, selectivity is a primary focus when utilising chiral materials for electrochemical sensing.<sup>43</sup> However, a major limitation is that the existing chiral recognition mechanisms are often oversimplified, with steric hindrance frequently being the primary explanation.<sup>43</sup> DA has flexible side chains that can adopt various conformations,<sup>44–46</sup> to fit the unique surface features of (6,5) SWCNTs. (6,5) SWCNTs have a helical structure, introducing asymmetry and additional surface features due to the difference in orientation of the edges.<sup>47–49</sup> This means DA can interact with multiple surface sites more favourably. Indeed, DA can form multiple molecular interactions with pure (6,5) SWCNTs.<sup>50</sup> On (6,6) SWCNTs, where the surface is more uniform and flatter, DA has fewer degrees of freedom to adapt and interact strongly, limiting the adsorption to primarily  $\pi$ - $\pi$  stacking interactions between the catechol ring and the flat SWCNT surface. Moreover, the higher curvature of (6,5) SWCNTs than (6,6) SWCNTs can affect how the molecules adsorbed on SWCNTs are “wrapped” around the surface. In contrast to DA, the organic molecules such as pyrene, porphyrins, and nucleobases are flat, resulting in a mismatch with the surface of SWCNTs.<sup>51</sup> Consequently, as the diameter of SWCNTs increases and the molecular surfaces of pyrene become more planar, there is a corresponding increase in the affinity of flat organic molecules for SWCNTs. When the shapes of the aromatic system and SWCNTs line up, their  $\pi$ -electron

interaction becomes more efficient, resulting in  $\pi$ - $\pi$  stacking interactions between the  $\pi$  electrons in SWCNTs and aromatic molecules.<sup>52</sup> Our observations and previous research using single-chirality SWCNTs suggest that certain chiralities can result in more favourable adsorption towards selected analytes. The interaction is affected by the flexibility of analytes, dimensions of single-chirality SWCNTs and their symmetrical *vs.* helical structure. Higher selectivity can be achieved if the electrode can be tailored to bind and react with the target analyte preferentially. Using single-chirality SWCNTs will provide a base for interpreting mechanisms of electrochemical sensors to detect biological molecules with well-defined selectivity and higher sensitivity.

To further investigate the role of SWCNTs' chirality in their electrochemical sensing mechanisms, it will also be interesting to explore other species with distinct chiral angles in future work. Additionally, to advance understanding, future research should leverage simulation studies to guide the design of chiral carbon-based materials. Techniques like Bayesian Optimization Structure Search (BOSS), which minimises human bias in identifying the most favourable adsorption configurations,<sup>53</sup> will be crucial in these efforts.

## 4. Conclusions

In conclusion, we fabricated electrochemical sensors using purified SWCNTs with specific chiralities (6,6) metallic and (6,5) semiconducting at well-defined concentrations. This ensured precise control over the material properties affecting sensor performance. Moreover, we employed multiple fabrication methods to produce surfactant-free electrochemical sensors. Removing surfactants was crucial to prevent interference with electrochemical characterisation and accurately evaluate the properties of SWCNTs based on chiralities.

Importantly, electron transfer processes of the ISR probe, DA revealed distinct electrochemical responses between (6,5) and (6,6) SWCNTs. The (6,5) SWCNTs exhibited adsorption-controlled processes, while (6,6) SWCNTs showed diffusion-controlled processes. This observation suggests that based on chirality, DA molecules interact differently and can adopt different conformations.

Consequently, our findings provide a standardised platform for SWCNT-based electrochemical sensing using well-characterized, surfactant-free, and single-chirality SWCNTs. These findings advance the understanding of how the chirality of SWCNTs affects electrochemical sensing mechanisms, highlighting the importance of material purity and surface conditions in sensor development and opening avenues for designing high-performance SWCNT-based biosensors with enhanced analytical capabilities.

## Author contributions

Ju-Yeon Seo: formal analysis, investigation, validation, visualisation, writing – original draft, writing – review & editing. Bahar



Mostafiz: formal analysis, investigation. Xiaomin Tu: formal analysis, data curation. Constantine Y. Khripin: formal analysis, data curation. Ming Zheng: writing – review & editing. Han Li: conceptualisation, formal analysis, funding acquisition, investigation, methodology, resources, supervision, writing – review & editing. Emilia Peltola: conceptualisation, funding acquisition, project administration, resources, supervision, writing – review & editing.

## Data availability

Data for this article, including raw data and analysed data sets by Origin software are available on Zenodo (<https://doi.org/10.5281/zenodo.14849004>).

## Conflicts of interest

There are no conflicts of interest to declare.

## Acknowledgements

This project has received funding from the European Union – NextGenerationEU instrument and is funded by the Research Council of Finland (RCF) under grant number 352 891. This project received funding from the RCF under grants number 321 996 and 352 899. H. L. gratefully acknowledges support from the Turku Collegium for Science, Medicine and Technology (TCSMT). The authors are thankful to the Materials Research Infrastructure (MARI) at the University of Turku for infrastructural facilities and Sari Granroth for performing the XPS measurements, and Nianxing Wang for performing the AFM measurements. The work was conducted under the #SUS-MAT umbrella.

## References

- S. Rathinavel, K. Priyadharshini and D. Panda, *Mater. Sci. Eng. B*, 2021, **268**, 115095.
- A. Sanati, M. Jalali, K. Raeissi, F. Karimzadeh, M. Kharaziha, S. S. Mahshid and S. Mahshid, *Microchim. Acta*, 2019, **186**, 773.
- C. B. Jacobs, M. J. Peairs and B. J. Venton, *Anal. Chim. Acta*, 2010, **662**, 105–127.
- N. Yang, X. Chen, T. Ren, P. Zhang and D. Yang, *Sens. Actuators, B*, 2015, **207**, 690–715.
- M. Feng, H. Han, J. Zhang and H. Tachikawa, *Electrochemical Sensors, Biosensors and their Biomedical Applications*, Elsevier, 2008, pp. 459.
- N. Punbusayakul, *Proc. Eng.*, 2012, **32**, 683–689.
- J. Wang, *Electroanalysis*, 2005, **17**, 7–14.
- M. Musameh, J. Wang, A. Merkoci and Y. Lin, *Electrochem. Commun.*, 2002, **4**, 743–746.
- S. Kang, M. Herzberg, D. F. Rodrigues and M. Elimelech, *Langmuir*, 2008, **24**, 6409–6413.
- S. Kang, M. Pinault, L. D. Pfefferle and M. Elimelech, *Langmuir*, 2007, **23**, 8670–8673.
- R. Saito, A. R. T. Nugraha, E. H. Hasdeo, N. T. Hung and W. Izumida, *Top. Curr. Chem.*, 2016, **375**, 7.
- W. Izumida, Quantum Effects in Carbon Nanotubes: Effects of Curvature, Finite-Length and Topological Property, in *Quantum Hybrid Electronics and Materials*, ed. Y. Hirayama, K. Hirakawa and H. Yamaguchi, Springer Nature Singapore, Singapore, 2022, pp. 123–148.
- R. Saito, G. Dresselhaus and M. S. Dresselhaus, *Physical Properties of Carbon Nanotubes, Published By Imperial College Press And Distributed*, World Scientific Publishing Co, 1998.
- M. S. Dresselhaus, G. Dresselhaus, R. Saito and A. Jorio, *Phys. Rep.*, 2005, **409**, 47–99.
- D. C. Ferrier and K. C. Honeychurch, *Biosensors*, 2021, **11**, 486.
- B. Dai, R. Zhou, J. Ping, Y. Ying and L. Xie, *TrAC, Trends Anal. Chem.*, 2022, **154**, 116658.
- C.-M. Tilmaciu and M. C. Morris, *Front. Chem.*, 2015, **3**, 59.
- A. Kaliyaraj Selva Kumar, Y. Lu and R. G. Compton, *J. Phys. Chem. Lett.*, 2022, **13**, 8699–8710.
- Q. Dong, M. Z. M. Nasir and M. Pumera, *Phys. Chem. Chem. Phys.*, 2017, **19**, 27320–27325.
- L. Chen, F. Chang, L. Meng, M. Li and Z. Zhu, *Analyst*, 2014, **139**, 2243–2248.
- L. Chen, S. Liu, F. Chang, X. Xie and Z. Zhu, *Electroanalysis*, 2017, **29**, 955–959.
- H. Zhu, F. Chang and Z. Zhu, *Talanta*, 2017, **166**, 70–74.
- Y. Yang, M. Li and Z. Zhu, *Talanta*, 2019, **201**, 295–300.
- W. Kuang, H. Luo and Z. Zhu, *Electrochim. Acta*, 2024, **487**, 144162.
- H. Li, G. Gordeev, O. Garrity, S. Reich and B. S. Flavel, *ACS Nano*, 2019, **13**, 2567–2578.
- H. Li, C. M. Sims, R. Kang, F. Biedermann, J. A. Fagan and B. S. Flavel, *Carbon*, 2023, **204**, 475–483.
- F. Yang, F. Yang, F. Yang, M. Wang, M. Wang, D. Zhang, D. Zhang, J. Yang, J. Yang, M. Zheng, M. Zheng, M. Zheng, M. Zheng, Y. Li and Y. Li, *Chem. Rev.*, 2020, **120**, 2693–2758.
- J. A. Fagan, *Nanoscale Adv.*, 2019, **1**, 3307–3324.
- M. Ishizaki, D. Satoh, R. Ando, M. Funabe, J. Matsui and M. Kurihara, *Adv. Mater. Inter.*, 2021, **8**, 2100953.
- S. Rantataro, I. Parkkinen, M. Airavaara and T. Laurila, *Biosens. Bioelectron.*, 2023, **241**, 115579.
- D. C. Harris, *Quantitative Chemical Analysis*, W. H. Freeman, 7th ed, 2007.
- E. Peltola, S. Sainio, K. B. Holt, T. Palomäki, J. Koskinen and T. Laurila, *Anal. Chem.*, 2018, **90**, 1408–1416.
- E. M. Pérez and N. Martín, *Chem. Soc. Rev.*, 2015, **44**, 6425–6433.
- C. Y. Khripin, X. Tu, J. Howarter, J. Fagan and M. Zheng, *Anal. Chem.*, 2012, **84**, 8733–8739.
- J. M. Harris, G. R. S. Iyer, D. O. Simien, J. A. Fagan, J. Y. Huh, J. Y. Chung, S. D. Hudson, J. Obrzut, J. F. Douglas, C. M. Stafford and E. K. Hobbie, *J. Phys. Chem. C*, 2011, **115**, 3973–3981.
- J.-L. Xu, R.-X. Dai, Y. Xin, Y.-L. Sun, X. Li, Y.-X. Yu, L. Xiang, D. Xie, S.-D. Wang and T.-L. Ren, *Sci. Rep.*, 2017, **7**, 6751.



- 37 K. Conley and A. J. Karttunen, *J. Phys. Chem. C*, 2022, **126**, 17266–17274.
- 38 H. Yang, L. Neal, E. E. Flores, A. Adronov and N. Y. Kim, *J. Surfactants Deterg.*, 2023, **26**, 607–622.
- 39 I. Soni and G. Kudur Jayaprakash, *J. Mol. Liq.*, 2023, **388**, 122737.
- 40 J. F. Cassidy, R. C. de Carvalho and A. J. Betts, *Electrochem*, 2023, **4**, 313–349.
- 41 K. Krukiewicz, M. Krzywiecki, M. J. P. Biggs and D. Janas, *RSC Adv.*, 2018, **8**, 30600–30609.
- 42 A. Kousar, I. Pande, L. F. Pascual, E. Peltola, J. Sainio and T. Laurila, *Anal. Chem.*, 2023, **95**, 2983–2991.
- 43 X. Niu, Y. Liu, R. Zhao, L. Wang, M. Yuan, H. Zhao, H. Li, X. Yang and K. Wang, *J. Mater. Chem. A*, 2024, **12**, 17073–17127.
- 44 A. Lagutschenkov, J. Langer, G. Berden, J. Oomens and O. Dopfer, *Phys. Chem. Chem. Phys.*, 2011, **13**, 2815–2823.
- 45 T. Yadav and V. Mukherjee, *J. Mol. Struct.*, 2018, **1160**, 256–270.
- 46 A. Chowdhury and P. C. Singh, *J. Chem. Sci.*, 2022, **134**, 25.
- 47 C. T. White and J. W. Mintmire, *J. Phys. Chem. B*, 2005, **109**, 52–65.
- 48 D. A. Areshkin, D. Gunlycke and C. T. White, *Nano Lett.*, 2007, **7**, 204–210.
- 49 H. Radinger, V. Trouillet, F. Bauer and F. Scheiba, *ACS Catal.*, 2022, **12**, 6007–6015.
- 50 C.-H. Yeh, Y.-J. Hsiao and J.-C. Jiang, *Appl. Surf. Sci.*, 2019, **473**, 59–64.
- 51 E. M. Pérez and N. Martín, *Chem. Soc. Rev.*, 2015, **44**, 6425–6433.
- 52 D. Umadevi, S. Panigrahi and G. N. Sastry, *Acc. Chem. Res.*, 2014, **47**, 2574–2581.
- 53 S. Sippola, M. Todorović and E. Peltola, *ACS Omega*, 2024, **9**, 34684–34691.

